Available online at www.sciencedirect.com
SCIENCE DIRECT®
Continental Shelf Research 25 (2005) 589–608
CONTINENTAL SHELF RESEARCH
www.elsevier.com/locate/csr

Variability in the spatio-temporal distribution and size-structure of phytoplankton across an upwelling area in the NW-Alboran Sea, (W-Mediterranean)

A. Reul[a,*], V. Rodríguez[a], F. Jiménez-Gómez[b], J.M. Blanco[a], B. Bautista[a], T. Sarhan[c], F. Guerrero[b], J. Ruíz[d,1], J. García-Lafuente[c]

[a]*Departamento de Ecología, Facultad de Ciencias, Universidad de Málaga, 29071-Málaga, Spain*
[b]*Departamento de Biología Animal, Biología Vegetal y Ecología, Facultad de Ciencias Experimentales, Universidad de Jaén, 23071 Jaén, Spain*
[c]*Departamento de Física Aplicada II, Universidad de Málaga, 29071 Málaga, Spain*
[d]*Area de Ecología, Facultad de Ciencias del Mar, Universidad de Cádiz, 11510 Puerto Real, Cádiz, Spain*

Received 28 November 2003; received in revised form 17 August 2004; accepted 24 September 2004

Abstract

A north–south transect crossing the quasi-permanent upwelling area and the front which usually occupies the north-western part of the Alboran Sea (Western Mediterranean) was sampled 16 times during four cruises, covering an annual cycle in order to study the coupling between hydrodynamics and phytoplankton spatial distribution. On a spatial scale, considerable changes in biomass, size-structure and composition of the phytoplankton community were found at both sides of the front. The upwelling area was characterized by higher cell abundance, higher mean integrated chlorophyll values, intense subsurface chlorophyll maximum (SSCM) dominated by the size fraction $>10\,\mu m$, as well as significantly less negative slopes of the size-spectra. Prokaryotic phytoplankton cells were more abundant in the oligotrophic waters off the front. These qualitative and quantitative differences of the phytoplanktonic spatial distribution were maintained in spite of the north–south displacement of the front that might occur even within days, in association with changes in position and size of the Western Alboran Gyre. On a temporal scale, the mean chlorophyll concentrations at the SSCM were similar in July and December (3.0 ± 0.4 and $3.5\pm1.0\,mg\,l^{-1}$ respectively), while abundance and biomass decreased in winter. The resulting lower C:Chl *a* and higher fluorescence $cell^{-1}$ ratio indicate photoacclimation in winter. Implications of the different SAS at both sides of the front on the fate of phytoplankton biomass and importance of field measurements for satellite image interpretation are discussed.

Keywords: NW-Alboran Sea; Upwelling; Front; Phytoplankton; Size-structure; Spatio-temporal variability; Photoacclimation

*Corresponding author. Departamento de Ecología, Facultad de Ciencias, Universidad de Málaga, 29071-Málaga, Spain. Tel.: 952137525; fax: 952132000.
E-mail address: areul@uma.es (A. Reul).
[1]Present address: Instituto de Ciencias Marinas de Andalucía, CSIC, 11510 Puerto Real, Cádiz, Spain.

0278-4343/$ - see front matter © 2004 Published by Elsevier Ltd.
doi:10.1016/j.csr.2004.09.016

1. Introduction

The Alboran Sea, together with the Gibraltar Strait, can be called the corridor of the Mediterranean Sea and, as such, has long been recognized as an oceanographic site of major interest (Prieur and Sournia, 1994). Hydrological observation (Gascard and Richez, 1985; Tintoré et al., 1988; Heburn and La Violette, 1990; García-Lafuente et al., 1998; Vargas-Yáñez et al., 2002, and references therein) and satellite images (Morel and André, 1991; Parada and Cantón, 1998; García-Górriz and Carr, 1999; Baldacci et al. 2001) reveal very complex temporal and spatial circulation patterns promoted by the exchange of Atlantic and Mediterranean waters through the Strait of Gibraltar. The large scale in the western Alboran Sea is dominated by a quasi-permanent western anticyclonic Gyre (WAG) enclosed and fed by the inflowing jet of superficial Atlantic water (AW), which undergoes changes in its properties as it progresses into the Mediterranean and becomes modified Atlantic water (MAW). The thermohaline characteristics of the Atlantic jet (AJ) are easily distinguishable from those of the adjacent waters to the north and generate a density front, which is revealed by salinity contrast throughout the year (Sarhan et al., 2000). Smaller scale analysis may show the existence of several mesoscale cyclonic eddies along the northern boundary of the WAG (Tintoré et al., 1991) and the presence of a concomitant almost permanent upwelling in the region (Cano, 1978; La Violette, 1984; Viúdez et al., 1996). This upwelling can be forced by several mechanisms, the two most important are the wind (westerly) driven upwelling and that due to the north–south excursion of the AJ-front (Sarhan et al., 2000). These local fertilization mechanisms enhance biological activity and raise controversy about the real productivity in oligotrophic areas as a whole.

In the Alboran Sea, in situ observational data and ocean colour data support the control exerted by above mentioned mesoscale circulation structures on the spatio-temporal distribution of phytoplankton biomass, primary production, the size-structure of phytoplankton communities, vertical particle fluxes, etc. (Rodríguez et al., 1998, 2001; García-Górriz and Carr, 1999; Ruíz et al., 2001; Morán and Estrada, 2001; Baldacci et al., 2001; Fabres et al., 2002; Arin et al., 2002; Echevarría et al., 2002). Biological data were always linked to physical forcing at the different scales resolved by the sampling design, emphasizing the necessity of spatially and temporally detailed in situ studies, which may contribute to the interpretation of satellite data and be fed back by ocean colour data.

The results presented in this paper undertake this objective through the analysis of the coupling between hydrodynamics and phytoplankton distribution in the northwestern Alboran Sea. In order to achieve this, the mesoscale and seasonal-subinertial temporal variability of phytoplankton size-distribution, abundance, biomass, and chlorophyll concentration were analyzed along a coastal-offshore transect crossing the almost permanent upwelling area, the front, and the northern edge of the WAG.

2. Material and methods

The study site is located in the NW-Alboran (Fig. 1). A section perpendicular to the shore (Estepona, Málaga) was visited on four consecutive times over 5-day cruises in April–July–December 1996 and May 1997 on board R/V Odón de Buen. These four cruises are labelled respectively as A, B, C and E in Table 1. During each cruise two replicate transects with chemical-biological sampling (labelled "a" and "b") were carried out. Before and after these two chemical-biological transects, physical (CTD) surveys (labelled "1" and "2") were carried out to study short-term dynamics of the front. The positions of the stations were dependent on the hydrological structure identified the day before, but on average the stations were placed every 8 km from the shoreline.

At each sampling station a CTD profile was carried out between 0 and 200 m. Eight sampling depths between 0 and 100 m were selected trying to collect water from the subsurface chlorophyll maximum (SSCM) and the 37.5 salinity layer, a cut-off value to delineate the boundary between

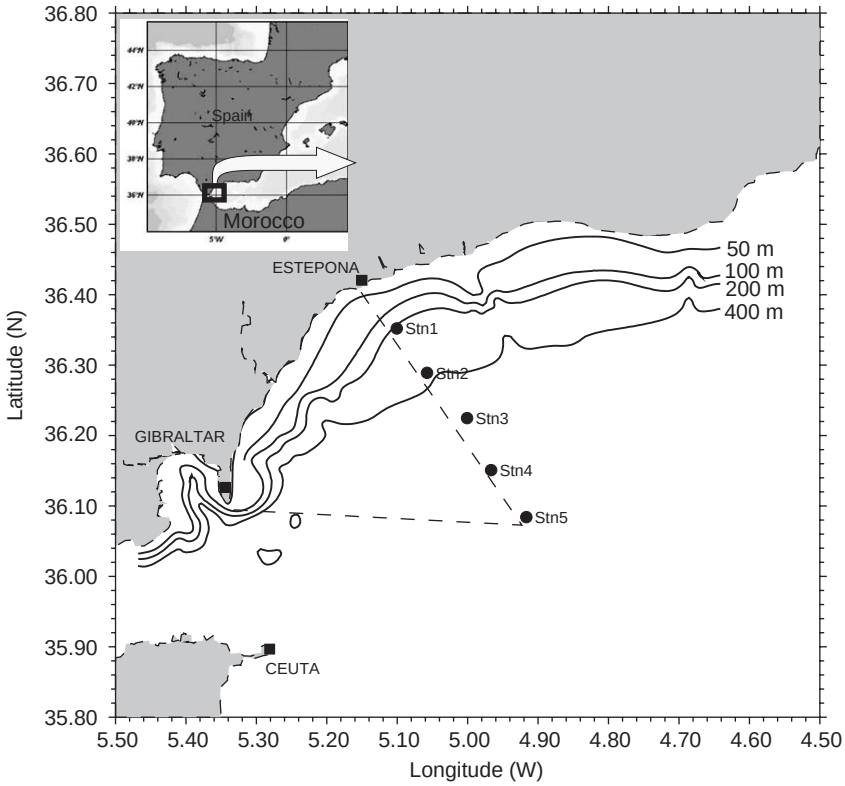

Fig. 1. Sampling area and the 5 station transect crossing the upwelling region sampled on four consecutive times over 5-day cruises in April (A), July (B) December (C) 1996 and May (E) 1997. Additional information about the actual hydrodynamic situation was provided by a CTD transect carried out one day before and after biological sampling (dotted line).

MAW, and the Mediterranean waters (MW) (Tintoré et al., 1991; García-Lafuente et al., 1999).

For each transect, the maximum gradient of salinity at 20 m depth was used to determine the position of the northern boundary of the AJ, the front (Sarhan et al., 2000). Wind direction and velocity at Tarifa, in the area of the Strait of Gibraltar, was provided by the Instituto Nacional de Meteorología (Spain). The incoming angle of the AJ the day of each cruise was obtained from currentmeter observations at the NE part of the Strait of Gibraltar available in CANIGO data-base.

Samples for nutrient analyses were kept in polyethylene vials rinsed with 5% HCL and immediately frozen (−20 °C). Nitrate, phosphate, silicate and nitrite concentrations were later measured with a Technicon AAII following Strickland and Parsons (1972).

Samples to estimate total Chl *a* (500 ml) were filtered on board through Whatman GF/F glass-fibre filters. For size-fractionated Chl *a* analyses, samples of 250 ml of water were successively filtered through 10 and 2 μm polycarbonate filters and GF/F glass-fibre filters. The filters were frozen at −20 °C and stored in dark prior to the Chl *a* analysis by fluorometry (Yentsch and Menzel, 1963) using a Turner Design-10 fluorometer.

Samples of 4.5 ml seawater were taken in cryotubes, fixed with glutaraldehyde (1% f.c.) and stored in liquid nitrogen (Vaulot et al., 1989) until the analysis with a Becton Dickinson FACScan flow cytometer. The combination of fluorescence signals (phycoerythrin and chlorophyll *a*) with measurements of forward and side light scatter, allowed the enumeration of cyanobacteria (*Synechococcus*), prochlorophytes (*Prochlorococcus*) and eukaryotic phytoplankton

Table 1
Survey (column #1), date (#2), distance of the front to the shore (#3), movement of the front between two successive surveys: (+) towards the shore, (−) towards the south (#4), horizontal salinity gradient at a depth of 20 m (#5)

Survey	Date	Dist. (km)	ΔK(m)	$\Delta S\,m^{-1} \times 10^{-5}$
A1	22/04/96	29.0		7.1
Aa	23/04-25/04/96#[a]	39.5	−10.5	6.7
Ab	26/04/96	27.3	+12.2	5.7
A2	27/04/96	19.4	+7.9	7.8
B1	07/07/96	26.9		5.6
Ba	08/07/-10/07/96#	19.9	+7	9.2
Bb	11/07/96	11.9	+8	13.6
B2	12/07/06	14.	−2.1	
C1	07/12/96	26.7		8.2
Ca	08/12/-09/12/96#	26.4	+0.3	5.1
Cb	10/12/96	36.4	−10	4.4
C2	11/12/96	26.7	+9.7	8.6
E1	02/05/97	35		5.0
Ea	03/05-04/05/97#	27.4	+7.6	5.5
Eb	05/05/97	>40	−(>)12.6	—
E2	06/05/97	>40		—

*The time interval required for the sampling of the 5 station transect during the Surveys Xa was <29 h.
[a]In Survey Aa only the sampling station 2, 3, 4 and 5 were considered for the calculation of the position of the front.

(Chisholm et al., 1988; Olson et al., 1990 and Li et al., 1992). Two separate analyses were carried out for *Prochlorococcus* and the remaining groups with different acquisition settings and sample volumes (0.24 and 0.4 ml) (see Reul et al., 2002 for details).

The forward scatter signal (FSC) of each cell was converted into cell volume by the equation $B_v = 10^{-1.78+0.0055\cdot FSC}$, where B_v is cell volume (μm^3) and FSC is the number of the forward scatter channel with E00 amplification (Jiménez-Gómez, 1995; Reul et al., 2002; Rodríguez et al., 2002). As for the size-fractionated chlorophyll, we discriminated three size-fractions of eukaryotic cells that correspond to "picoplankton" (<2 μm ESD), "nanoplankton" (2–10 μm ESD) and "large nanoplankton" (10∼20 μm ESD). However, cell size estimation by FC is influenced by the light history of the cells, which was not considered in the present study, and cell size estimates in surface water might be greater than below the mixed layer (Green et al., 2003). This uncertainty increases with cell size, but good agreement between FC and IA size-abundance-spectra (SAS) (Fig. 2) gives confidence to the nanoplankton estimates derived from FC measurements.

Additional water samples were placed in 125 ml darkened glass bottles and fixed with Lugol's solution (2% f.c.). At the laboratory, the analysis of phytoplankton was performed at two depths (surface and SSCM) following the method of Utermöhl (1958). At least 400 cells were counted and measured at 400 ×, 200 × and 100 × with the help of an inverted microscope connected to a VIDS-IV video-interactive Image Analyzer. Biovolume for each individual organism was estimated as a revolution volume according to an ellipsoidal or cylindrical shape. Cells were identified into broad groups such as diatoms, flagellates and dinoflagellates.

Complete SAS were elaborated by a combination of the size-spectra derived from FC and IA measurements (Fig. 2). Size classes were established on an octave ($\log_2$) scale basis scale. Then the $\log_{10}$ of the abundance was represented versus

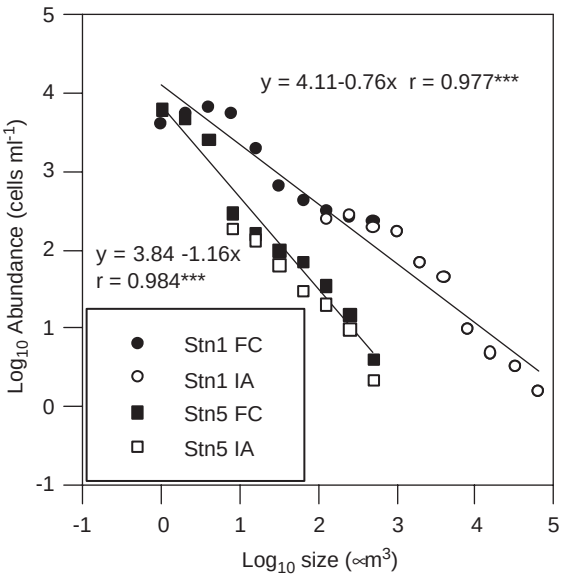

Fig. 2. Phytoplankton size-spectra between 1 and 200 μm ESD obtained by combination of the size-spectra derived from FC measurements (black symbols) and IA (open symbols). Upwelling area (Stn 1, circles) and off the front (Stn 5, squares) at surface during Survey (Ba) in July 1996.

Table 2
Conversion formulae used to estimate plankton biomass

Biological group	Formulae	Reference
Synechococcus	$B_m = 0.25\cdots$cell	Kana and Glibert, 1987
Prochlorococcus	$B_m = 0.053\cdots$cell	Morel et al., 1993
Eukariotic phytoplankton $<15\,\mu m$	$B_m = 0.433\cdots(B_v)^{0.863}$	Verity et al., 1992
Dinoflagellates&others $>15\,\mu m$	$B_m = 0.433\cdots(B_v)^{0.864}$	Menden-Deuer and Lessard, 2000
Diatoms $>15\,\mu m$	$B_m = 0.288\cdots(B_v)^{0.811}$	Menden-Deuer and Lessard, 2000

B_m is biomass (pgC), B_v is Biovolume (μm^3).

the $\log_{10}$ of the lower limit of the corresponding octave size class. Both methodologies (FC and IA) overlap in the size classes between 128–2048 μm^3 (6–16 μm ESD). A value of 15 μm ESD was selected as the limit between both methodologies in the complete SAS. Only size classes with an original count of more than 5 cells were considered.

To calculate the ratio of biomass to Chl *a* (C:Chl *a*) the cell volume of eukaryotic phytoplankton was converted into carbon equivalent using published conversion factors and equations shown in Table 2. For *Prochlorococcus* and *Synechococcus* we used a carbon conversion factor *per* cell. Abundance and cell size of phytoplankton $<15\,\mu m$ ESD were analysed by FC and phytoplankton $>15\,\mu m$ ESD by IA.

3. Results

In Table 1 we present, for each survey, the distance of the front to the shore and the north–south movements of the front between two successive surveys. Zonal wind component, which provides information about wind-driven upwelling (WU), and the incoming angle under which the AJ comes into the Alboran Sea, related to the importance that jet drift upwelling events (DU) might have, are shown in Fig. 3. Among the several cruises, the summer and winter cruises (B and C) depict two very contrasted situations: northward *vs.* southward drifts of the front; easterlies *vs.* westerlies prevailing winds, and increasing *vs.* decreasing incoming angles, respectively. These are the reasons for presenting the results from cruises B and C in some detail as representative examples of these two aforementioned situations.

3.1. Hydrology and nutrients

Vertical sections of salinity, temperature and nitrate of the first transect of cruise B (July) are shown in Fig. 4. The isohalines rise towards the surface from the open sea to the shore, the isohaline 37.0 reaching the surface at Stn 1 (~8 km offshore) from a depth of 90 m at Stn 4. The front, defined by a salinity gradient of $9\times10^{-5}\,m^{-1}$ at a depth of 20 m, was located 20 km offshore (Table 1), and located between stations 2 and 3. The strong summer thermocline found at the outermost station (Stn5) gradually weakens towards the coast, a fact that suggests the presence of colder, Mediterranean water close to the coast. It is important to note that the westerlies blowing previously to cruise B sharply changed to very strong easterlies during the cruise (Fig. 3). So, the upwelling at the most coastal stations (in apparent contradiction with easterlies) may be the residual of the favourable previous conditions. Several important changes occur along the two replicate transects (Ba and Bb, Table 1 and Fig. 3): (a) shoreward movement of the front from 20 to 12 km, which is in agreement with an increase of the incoming angle of the AJ between 7–12th, July; (b) the intrusion of more surface AW (salinity <36.5; not shown) that fills the upper water column from a depth of ~90 m at station 5 to a depth of ~20 m at station 2, and (c) generalized sinking of the cut-off isohaline 37.5 and intensification of the thermal stratification at the surface of

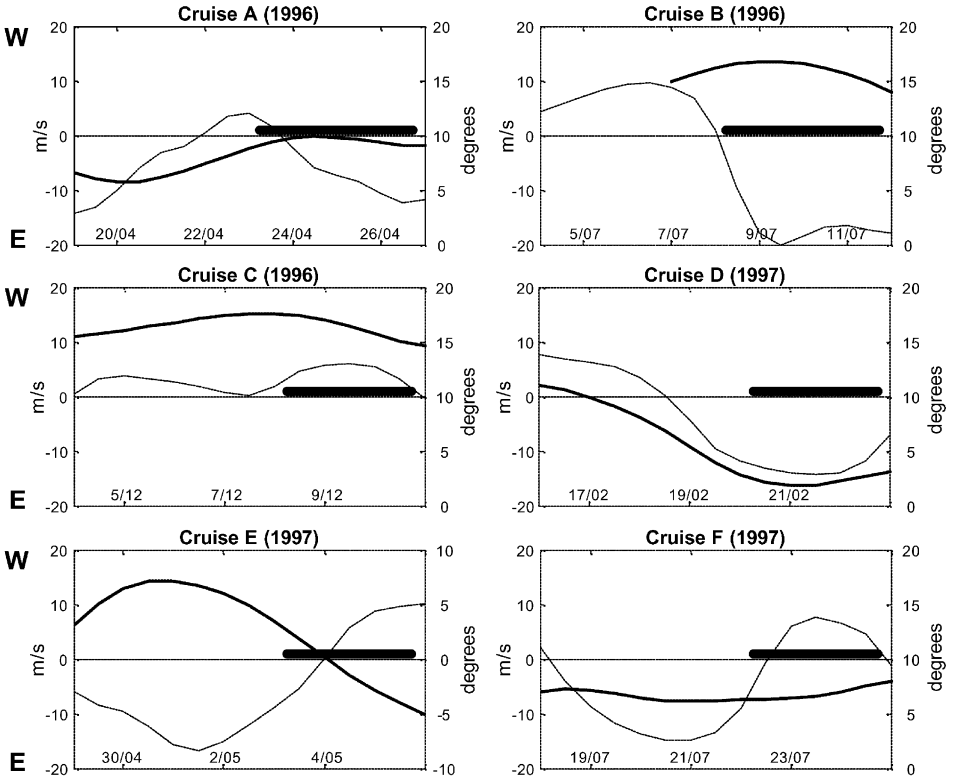

Fig. 3. Component of mean E-W wind at Tarifa ($m\,s^{-1}$, left scale), positive values indicate Westerlies and negative values Easterlies (thin line). Mean entrance angle (degrees, right scale) of the AJ at the NE of the Strait of Gibraltar (36°02.4N, 5°23.7W) at 40 m depths (bold line). The front moves towards the north if the angle increases (positive counterclockwise) and vice versa. The sampling periods of the cruise is indicated by the bold horizontal line.

the two outermost stations (not shown). All these variations are in concordance with daily sea surface temperature satellite images available at the German Remote Sensing Data Centre (DLR), http://isis.dlr.de.

The nitrate concentration reached minimum values ($<0.5\,\mu M$) in the upper 50 m at station 5, and also in the upper 20 m of the upwelling area (Stn1 and Stn2, Fig. 4). While the surface nitrate minimum located off the front coincided with the presence of nutrient impoverished AW and strong thermal stratification, it was difficult to quantify the availability of nutrients at the surface nitrate minimum in the upwelling area without any measurements of upwelling rates. The distribution of phosphate and silicate concentrations followed the same pattern as nitrate concentration.

During cruise C (December), the salinity values measured successively in Ca and Cb surveys suggest the existence of a front between station 3 and 4 (26 km) and between station 4 and 5 (36 km), respectively (Table 1, Fig. 5). The isohaline 37.0 reached the surface 15 km offshore in Ca and 26 km offshore in Cb (not shown). So, the salinity values at the surface waters in the upwelling area are always 37.5–37.0, a range value associated to the Atlantic–Mediterranean interface (AMI). The movement of the front means southward drifts of about 10 km in two days (Table 1) and causes an expansion of the upwelling area.

Several factors enhance the upwelling: (a) westerlies that induce upwelling by Ekman transport, (b) decrease of the incoming angle of the AJ (Fig. 3) and (c) weak thermal stratification (Fig. 5).

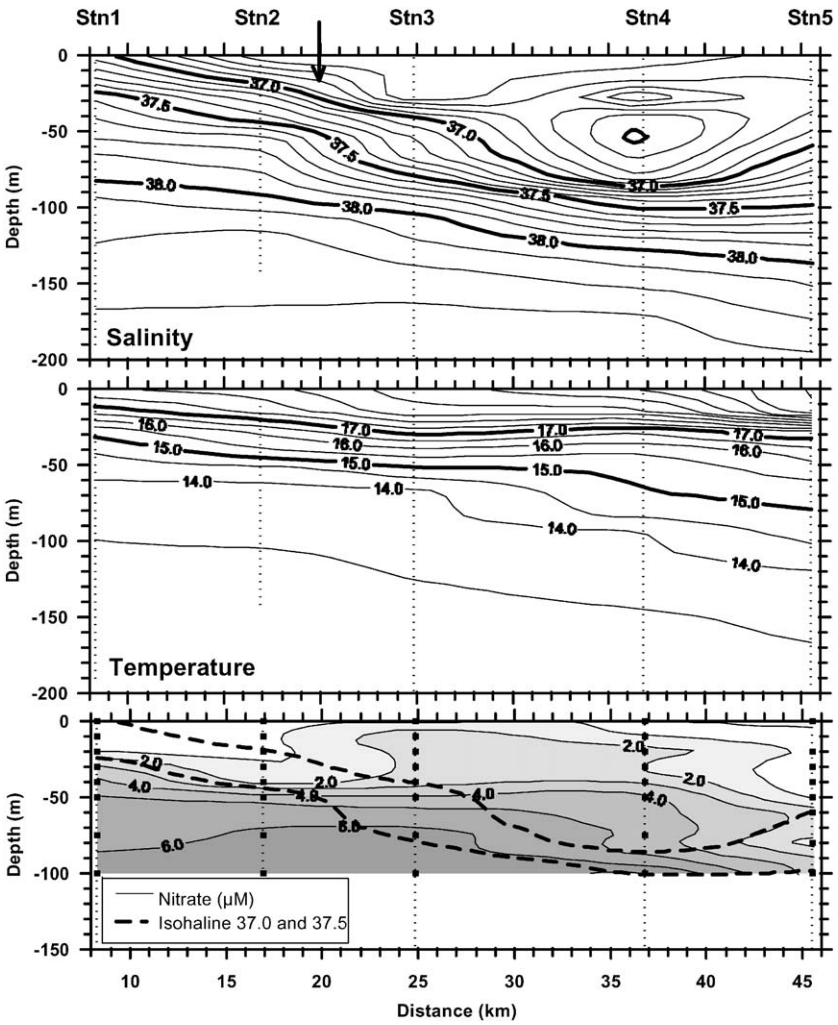

Fig. 4. Salinity, temperature (°C) and nitrate concentration (μM) of the survey Ba in July 1996. On the nitrate plot the AMI (37.0–37.5 isohalines) is indicated by dotted lines. The vertical arrow indicates the position of the front.

The low nutrient concentration off the front persists in December (Fig. 5) and the smallest concentration of nitrates was also found in the upper 20 m of the outermost station. In contrast to July, nutrient concentration did not decrease at the surface of the upwelling area. Concentrations of nitrate, phosphate and silicate in the water column were always greater than 1.5, 0.12 and 1.8 μM, respectively.

3.2. Spatial distribution of phytoplankton

3.2.1. Chlorophyll

At survey Ba (July), a marked SSCM ($3.39\,\mu g\,l^{-1}$) was centred at a depth of 30 m between the sloping up isohalines 37.5 and 37, occupying the area from the shoreline to the front (Stn 1 and Stn 2, Fig. 6). Chlorophyll concentration in particles $>10\,\mu m$ accounted for 87% of

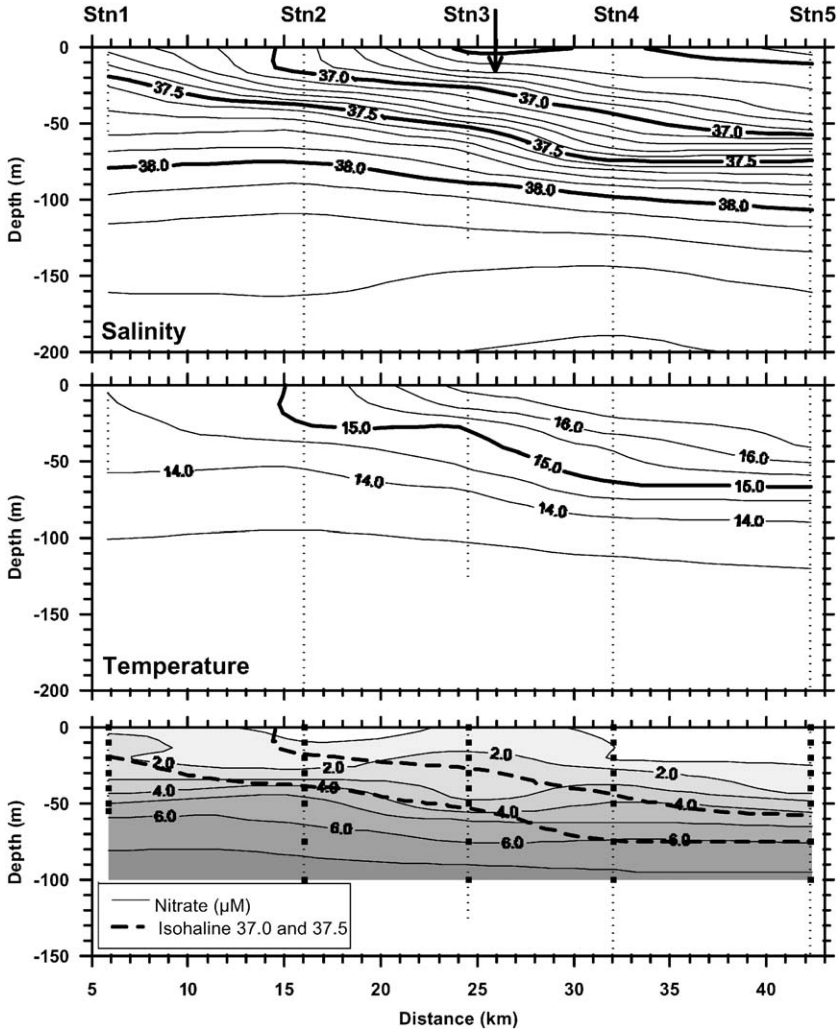

Fig. 5. Salinity, temperature (°C) and nitrate concentration (μM) of the survey Ca in December 1996. AMI limits and vertical arrow as in Fig. 4.

total Chl *a*, while Chl *a* $<10\,\mu m$ were one order of magnitude lower. A weaker and deeper chlorophyll maximum ($0.23\,\mu g\,l^{-1}$, 60 m deep) was found off the front (Stn 5), which was dominated by the $<2\,\mu m$ size-fraction (87%) because of the marked decrease in the concentration of chlorophyll $>10\,\mu m$ in this area.

The depicted spatial pattern persists in winter (cruise C, December, Fig. 7). It is worth mentioning the expansion of the area of SSCM associated to the southward movement of the front and its deepening at the frontal region. Also, maximum Chl *a* concentrations are similar ($3.5\,\mu g\,l^{-1}$, Fig. 7) and even greater ($5.0\,\mu g\,l^{-1}$, survey Cb, not shown) than those measured in July, and Chl *a* $>10\,\mu m$ size-fraction is the main contributor to the total Chl *a* (60% on average; 89% at the SSCM). Mean Chl *a* concentration at the SSCM was highest during the winter cruise ($3.5\pm1\,\mu g\,l^{-1}$ in the upwelling area and $1.0\pm0.2\,\mu g\,l^{-1}$ off the front, Table 3). The same pattern was observed for mean integrated Chl *a* concentration in the upwelling area ($148.9\pm63.1\,mg\,m^{-2}$) and off the front ($58.3\pm30.3\,mg\,m^{-2}$, Table 3).

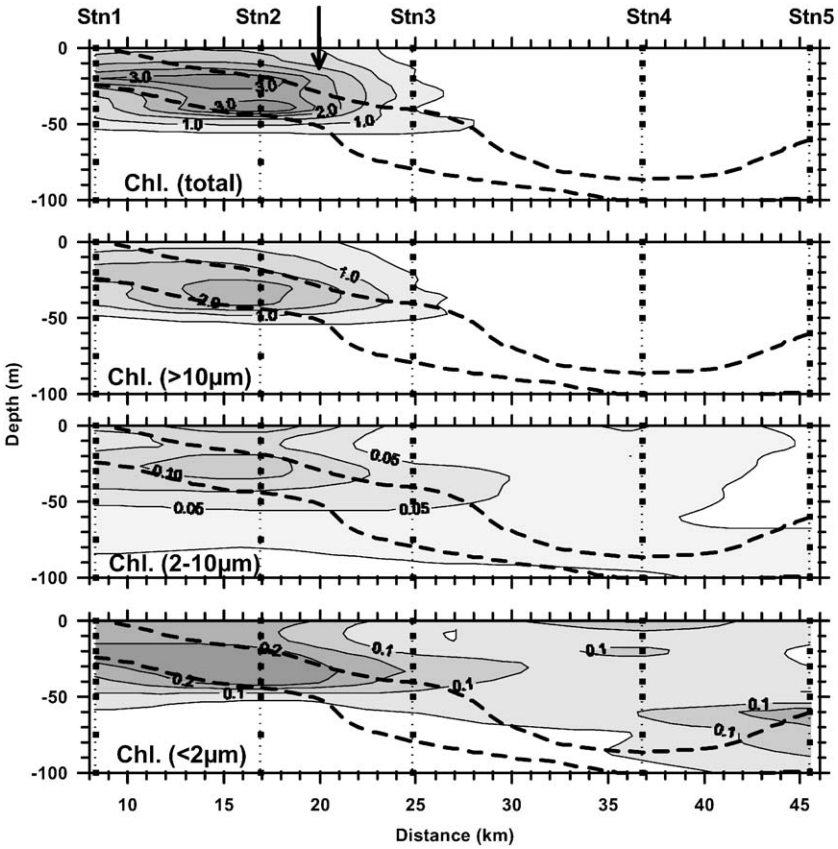

Fig. 6. Chlorophyll *a* ($\mu g\,l^{-1}$) total and size-fractionated (>10 µm, 2–10 µm and <2 µm), of the survey Ba in July 1996. AMI limits and vertical arrow as in Fig. 4.

Considering all the cruises, the mean concentrations of chlorophyll at the SSCM, the relative contribution of the size fraction >10 µm and the mean integrated Chl *a* values were significantly higher ($p<0.05$, paired *t*-test) in the upwelling area ($2.65\pm0.8\,\mu g\,l^{-1}$, $n=4$; $70\pm10\%$; $104.9\pm34.0\,mg\,m^{-2}$, $n=4$) than off the front ($0.63\pm0.3\,\mu g\,l^{-1}$, $n=4$; $41\pm13\%$; $37.5\pm17.2\,mg\,m^{-2}$, $n=4$). Also, a significant relationship ($r^2=0.62$, $p<0.001$) existed between the surface and 50 m integrated values of Chl *a*.

3.3. Phytoplankton abundance and biomass

In agreement with the fractionated Chl *a* distributions observed in summer (survey Ba), the two larger eukaryotic size classes determined by flow cytometry (2–10 µm and 10~20 µm), but particularly the cells >10 µm (FC and IA) reached highest abundance in the more intensive and shallower SSCM in the upwelling area (Fig. 8). In terms of biomass, diatoms >15 µm ESD were the major contributor to phytoplankton biomass (51%, Table 5).

Eukaryotic picoplankton (<2 µm) showed similar abundance at both sides of the front ($\sim1\times10^4$ cells ml^{-1}). On the contrary, prokaryotic picoplankton (*Prochlorococcus* and *Synechococcus*) reached highest abundances off the front, associated to the impoverished MAW. Although *Synechococcus* was the most abundant cell and the main contributor to the biomass (48%) at the weaker and deeper SSCM off the front observed in Survey Ba (July, Figs. 6 and 8), eukaryotic

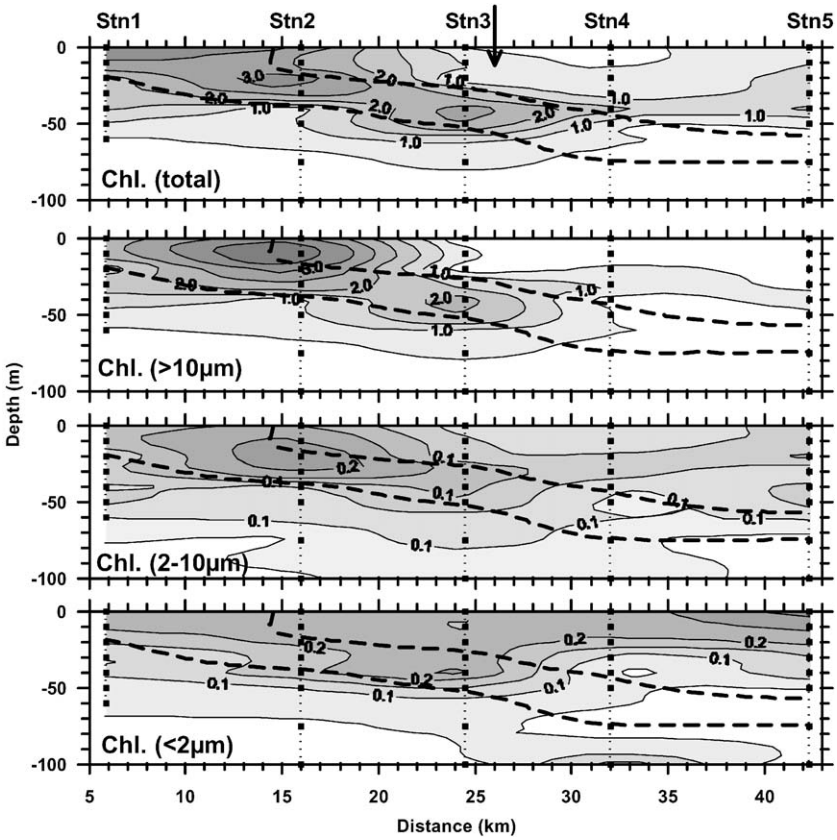

Fig. 7. Chlorophyll *a* ($\mu g\,l^{-1}$) total and size-fractionated (>10 µm, 2–10 µm and <2 µm), of the survey Ca in December 1996. AMI limits and vertical arrow as in Fig. 4.

Table 3
Mean chlorophyll *a* concentration ($\mu g\,l^{-1}$) at the SSCM and mean integrated (0–100 m) chlorophyll *a* concentration ($mg\,m^{-2}$) in the upwelling area and off the front

Cruise	Chlorophyll a ($\mu g\,l^{-1}$) at the MSSC						Integrated Chlorophyll *a* 0–100 m ($mg\,m^{-2}$)					
	Upwelling area			Off the front			Upwelling area			Off the front		
	Mean	sd	*n*	Mean	sd	*n*	Mean	sd	*n*	Mean	sd	*n*
A	2.4	0.7	7	0.4	0.3	3	98.3	26.9	7	25.7	5.2	3
B	3.0	0.4	3	0.4	0.3	7	105.9	38.1	3	21.2	9.0	7
C	3.5	1.0	7	1.0	0.2	3	148.9	63.1	6	58.3	30.3	3
E	1.6	0.4	8	0.8	0.1	2	66.4	15.2	8	44.9	31.7	2

Standard deviation (sd) and number of samples (*n*).

picoplankton was the main contributor to Chl *a* concentration.

The spatial pattern observed in survey Ba (Fig. 8): large eukaryotic cells in the upwelling area and prokaryotic picoplankton off the front was maintained in all cruises in spite of considerable short-term variability of the position of the front. These findings suggest that the front acts as a physical frontier for phytoplankton assemblages.

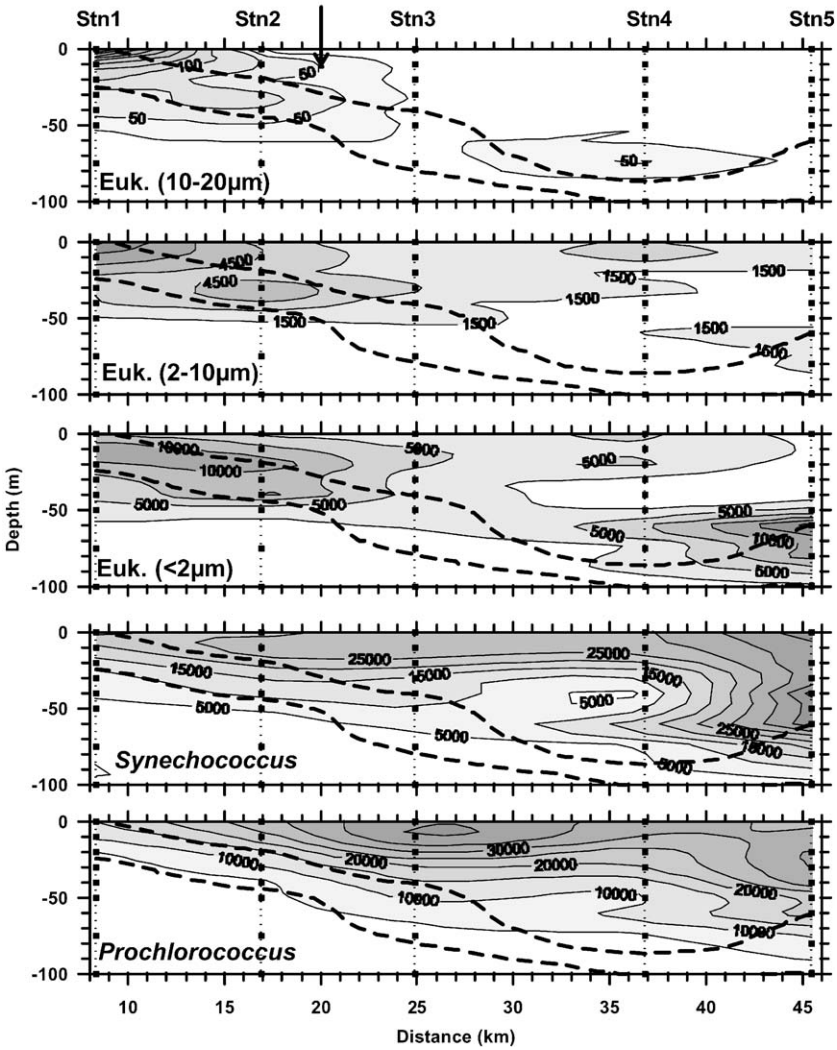

Fig. 8. Abundance (cells ml^{-1}) of eukaryotic phytoplankton size-fractions (10~20 µm, 2–10 µm and <2 µm) and prokaryotic picophytoplankton (*Synechococcus* and *Prochlorococcus* of the survey Ba in July 1996. AMI limits and vertical arrow as in Fig. 4.

On the temporal scale, the main change to emphasize is the decrease in the biomass at the SSCM in December (Table 4) which is not accompanied by a proportional decrease of Chl *a*. In fact, the highest values of the mean fluorescence per cell of samples between 0-100 m (Table 5) were observed during the December (C) cruise, which were significantly higher than the fluorescence cell^{-1} values observed in July (cruise B).

3.3.1. C:Chl a ratios

The C:Chl *a* ratio was calculated for two depths (surface and SSCM) for the first transect of the four cruises (Aa, Ba, Ca and Ea, Table 6). The average C:Chl *a* ratio was higher than the value generally accepted (50) and it was affected by a very high dispersion of the data. The values were higher at surface waters than at the SSCM in all the surveys. On a temporal scale, lowest average C:Chl a ratio was observed in

Table 4
Biomass (mgC m^{-3}) and relative contribution of differentiated taxonomic groups and size fractions at the SSCM

Survey	Station	Relative position	Biomass (mgC m^{-3})	Proc (%)	Syn (%)	Euk. <2 (%)	Euk. 2–15 (%)	Diat. >15 (%)	Dinof. >15 (%)
Aa	1	U	251	0.1	4.1	0.8	65.7	25.5	3.8
Aa	2	U	223	0.2	4.4	2.3	48.0	41.1	4.0
Aa	3	U	193	0.0	4.1	2.0	34.1	46.8	12.9
Aa	4	U	189	0.1	3.3	1.7	61.9	18.4	14.7
Aa	5	O	57	0.2	12.5	5.0	70.5	6.8	5.1
Ba	1	U	126	0.2	2.5	4.2	49.1	37.2	6.8
Ba	2	U	168	0.3	2.4	3.3	37.0	51.2	5.9
Ba	3	O	38	2.1	9.9	6.1	38.6	36.1	7.3
Ba	4	O	28	4.1	17.1	7.9	39.4	26.0	5.4
Ba	5	O	24	7.4	48.3	3.6	33.6	2.4	4.8
Ca	1	U	44	0.1	0.6	0.2	45.9	45.9	7.2
Ca	2	U	111	0.2	0.7	0.4	64.3	30.6	3.8
Ca	3	U	99	0.2	0.7	0.3	46.6	44.8	7.5
Ca	4	O	29	2.2	3.1	3.0	79.1	10.7	1.9
Ca	5	O	39	1.7	2.9	2.3	73.2	6.3	13.6
Ea	1	U	96	0.0	2.1	2.0	30.8	51.8	13.2
Ea	2	U	93	0.0	2.6	2.5	29.1	55.4	10.3
Ea	3	U	104	1.2	7.9	7.2	50.8	27.7	5.3
Ea	4	O	118	0.6	2.9	5.2	45.6	10.8	35.0
Ea	5	O	53	1.7	7.9	7.6	65.3	15.2	2.2

Survey, sampling station, and relative position to the front (U) upwelling area and (O) off the front are indicated in the first three columns.

Table 5
Comparison of the mean channel of fluorescence >650 nm $cell^{-1}$ ratio of FC measurements analysed with a setting of 300 mV

Fluorescence $cell^{-1}$							
Cruise	Median	25%	75%	n	H	df	p
A	421.2	402.1	445.7	70	13.2	3	<0.01
B	412.4	379.4	430.2	80			
C	438.6	403.5	449	79			
E	416.1	383.8	441.9	81			

All samples between 0–100 m depths of each cruise (A, B, C, E) were considered in the Kruskal–Wallis one way analysis of variance on ranks. The pairwise multiple comparison (Dunn's Method) depict that the median fluorescence >650 nm $cell^{-1}$ ratio of cruise C (December) is significantly higher than the median of cruise B (July).

December (Ca), either at the surface or at the SSCM.

The results of a variance analysis on log transformed C:Chl *a* ratio (Table 7) corroborate those observations. It show differences between a) the surface (2.0) and the SSCM (1.8); and b) among cruises (April, July, December, May): a post hoc test of Student-Newman–Keuls Method reveal that the log C:Chl *a* ratio in December is significantly lower (1.6) than the log C:Chl *a* ratio of the other three cruises (2.1 in April and July; 2.0 in May). However, no difference exists between the log C:Chl *a* ratio at both sides of the front.

3.4. Phytoplankton size-structure

Independent of the survey (season) and vertical position (0 m, SSCM), the slope of the combined

Table 6
Mean C:Chl *a* ratio, standard deviation (sd) and number of samples (n) at surface and the SSCM

Cruise	Surface			SSCM		
	Mean	sd	*n*	Mean	sd	*n*
Aa	183.7	66.6	5	96.2	28.4	5
Ba	155.4	103.8	5	147.6	142.9	5
Ca	60.5	36.9	5	32.7	4.1	5
Ea	134.3	59.9	5	79.8	31.1	5

Table 7
Two-way ANOVA on log transformed C:Chl *a* ratio

Source of variance	DF	SS	MS	*F*-value	*P*-value
Space (surface-MSSC)	1	0.37	0.37	6.40	0.016
Time (April, July Dec, May)	3	1.48	0.49	8.55	0.000
Interaction (space-time)	3	0.05	0.02	0.29	0.834
Residual	32	1.85	0.06		
Total	39	3.74	0.10		

Table 8
Regression and comparison of combined SAS at both sides of the front of each Cruise

Survey	Relative position	SAS (*n*)	Surface (0 m) SSCM	Intercept (a)	Std	Slope (b)	Std	R^2	*P*	Ancova a	Ancova b
Aa	U	4	0 m	3.868	0.078	−0.635	0.030	0.881	***	***	***
Aa	O	1	0 m	3.894	0.100	−0.930	0.043	0.975	***		
Aa	U	4	SSCM	3.812	0.066	−0.628	0.025	0.910	***	**	***
Aa	O	1	SSCM	4.037	0.148	−0.982	0.060	0.954	***		
Ba	U	2	0 m	3.987	0.078	−0.730	0.030	0.954	***	***	***
Ba	O	3	0 m	3.728	0.074	−0.911	0.032	0.955	***		
Ba	U	2	SSCM	3.774	0.086	−0.608	0.032	0.922	***	***	***
Ba	O	3	SSCM	3.403	0.077	−0.794	0.030	0.940	***		
Ca	U	3	0 m	3.206	0.098	−0.536	0.038	0.819	***	*	***
Ca	O	2	0 m	3.498	0.129	−0.805	0.061	0.879	***		
Ca	U	3	SSCM	3.033	0.110	−0.513	0.040	0.777	***	n.s	***
Ca	O	2	SSCM	3.468	0.106	−0.757	0.046	0.913	***		
Ea	U	3	0 m	3.567	0.092	−0.667	0.035	0.887	***	*	n.s
Ea	O	2	0 m	3.516	0.099	-0.791	0.037	0.926	***		
Ea	U	3	SSCM	3.564	0.078	−0.665	0.027	0.924	***	*	***
Ea	O	2	SSCM	3.788	0.067	−0.807	0.023	0.975	***		

Survey (column #1). Relative position to the front: upwelling Area (U) and off the front (O) (column #2), number of SAS considered (column #3). Vertical position of the SAS: surface (0m) and SSCM (column #4), intercept (a) and standard error (column #4&5), slope and standard error (column #6&7) of the SAS, R^2 and significance of the regression model (column #8&9), comparison of the intercept (a) and slope (b) (column #10&11) $*p<0.05$,$**p<0.01$, $***p<0.001$.

SAS was always less negative in the upwelling area than off the front (Table 8). Thus, the relative contribution of big cells to the phytoplankton biomass was significantly higher in the upwelling area than off the front throughout the year.

The slopes of the SAS of the four surveys were positively correlated (flatter, or less negative) with salinity ($r = +0.645$, $n = 40$, $p < 0.001$), and negatively correlated (steeper, or more negative) with temperature ($r = -0.645$, $n = 40$, $p < 0.001$). Furthermore, a negative correlation between the water column stability (Brunt–Väisälä–frequency) in the first 100 m and the slope of the size-spectra was also found ($r = -0.404$, $n = 38$, $p < 0.05$). Thus, the SAS become flatter as potential nutrient availability increases (increase of salinity and decrease of temperature) and water stability decreases, giving support to the increased relative contribution of bigger cells to the phytoplankton biomass increased in the upwelling area, and driving presumably to a more efficient canalization of the biomass to the seafloor or exploitable fish stocks.

4. Discussion

The northwestern part of the Alboran Sea around 5°W usually presents the highest values of chlorophyll and primary production as well as the lowest in situ and satellite sea surface temperature in the basin (Rodríguez et al., 1997; Rodríguez et al., 1998; García-Górriz and Carr, 1999; Morán and Estrada, 2001; Ruíz et al., 2001; Baldacci et al., 2001; Arin et al., 2002). The northern edge of the incoming AJ is the southern boundary of the upwelling area in such a way that the strong gradient properties between water northwards and inside the jet produces one of the most intense fronts of the Mediterranean Sea (Sarhan et al., 2000). The front position fluctuates in a north–south direction in connection with the velocity variation of the inflow through the Strait of Gibraltar and with the internal hydraulics of the Strait (Bormans and Garret, 1989; Bryden and Kinder, 1991) that affects the position, size and shape of the WAG (La Violette,1984; García-Lafuente et al., 1998).

In this study, the sloping up of the isohalines towards the coast and the consequent nutrient enrichment of the surface waters always produced a marked contrast between the coastal upwelled waters and water off the front, with the greatest values of phytoplankton biomass in the upwelled water forced mainly by wind (westerly) stress and the southward drifting of the AJ. However, other mechanisms have been suggested to explain similar phytoplankton distribution: the ageostrophic upward velocities in the same region and mixing processes tidally induced along the Strait that periodically fertilize the upper layer that enters into the Alboran Sea (Ruíz et al., 2001; Echevarría et al., 2002).

Nutrients furnished by upwelling are consumed by phytoplankton and the measured concentration is low. Without any measurements of upwelling rates, an estimation of the potential nitrate concentration in upwelled water was calculated using the salinity values as a tracer for mixing between (a) surface, poor nutrient water off the front and (b) deep, nutrient rich, saline and potentially upwelled water (Minas et al., 1986). The resulting nitrate concentration at 10 m depth in the upwelling area of Survey Ba is $>1\,\mu M$ and suggests a fast incorporation of nitrate by phytoplankton which lead to concentration $<1\,\mu M$ in the first 20 m in the upwelling area (Fig. 4).

Nitrate concentration was negatively correlated with abundance of cells $>2\,\mu m$, but no relationship was found with phosphate (Table 9). In addition, the median nitrate:phosphate ratio (N:P) above the nutricline was smaller than the Redfield ratio of 16 for optimal phytoplankton growth (Table 10), suggesting a main role of nitrate in the regulation of phytoplankton growth, as generally accepted for most of the world's ocean (Dugdale and Goering, 1967; Krom et al., 1991; Fanning, 1992; among others). Even though this observation is the expected result from the assumptions of (a) nitrogen-limited growth in the inflowing Atlantic water and (b) a faster recycling of phosphorous than nitrogen (Thingstad et al., 1998), is however surprising because several studies carried out in the western Mediterranean have shown N:P ratios higher than 16:1, indicating that P is the principal limiting nutrient during all or part of the year (Thingstad et al., 1998; Krom et al., 1991; Morán et al., 2001).

In fact, 85% of our samples below the nutricline showed a N:P ratio higher than 16, supporting the usual trend of deep Mediterranean waters to be

Table 9
Correlation (Spearman Rank Order) between the abundance of phytoplanktonic groups $<20\,\mu m$ ESD, and physical (temperature, salinity, depth of the AMI (isohaline 37.5), and the depth average of N^2 (Brunt-Väisälä-frequency) between the bottom of the nutricline and the sample) and chemical variables (nitrate, nitrite, phosphate and silicate), as well as total and size-fractionated chlorophyll *a* concentrations

	Proc. (cells ml^{-1})			Syn. (cells ml^{-1})			Euk $<2\,\mu m$ (cells m^{-1})			Euk2–10 μm (cells m^{-1})			Euk10–20 μm (cells m^{-1})		
	r	*n*	*p*	*r*	*n*	*p*	*r*	*n*	*p*	*r*	*n*	*p*	*r*	*p*	*n*
Temperature (°C)	0.55	277	***	0.43	300	***	0.27	299	***	−0.29	299	***	−0.41	***	299
Salinity	−0.50	277	***	−0.17	300	**	−0.11	299	n.s	0.10	299	n.s	0.45	***	299
N^2 Depth average (bottom nutricline−sample)	0.22	277	***	0.33	300	***	0.27	299	***	−0.16	299	**	−0.10	n.s	299
Distance to AMI (37.5)	0.41	277	***	0.15	300	*	0.03	299	n.s	−0.15	299	*	−0.45	***	299
NO_3^- (μm)	0.09	263	n.s	−0.31	283	***	−0.30	282	***	−0.33	282	***	−0.31	***	282
NO_2^- (μm)	−0.05	274	n.s	−0.19	296	***	−0.11	295	n.s	−0.16	295	**	−0.07	n.s	295
PO_4^{3-} (μm)	0.08	273	n.s	−0.36	296	***	−0.34	295	***	−0.09	295	n.s	−0.06	n.s	295
SiO_4^{4-} (μm)	0.03	274	n.s	−0.45	297	***	−0.31	296	***	−0.19	296	**	−0.22	***	296
Proclorococcus (cells m^{-1})															
Synechococcus (cells m^{-1})	0.30	277	***												
Euk. $<2\,\mu m$ (cells m^{-1})	0.12	276	***	0.61	299	***									
Euk. 2–10 μm (cells m^{-1})	−0.15	276	*	0.17	299	**	0.45	299	***						
Euk. 10–20 μm (cells m^{-1})	−0.45	276	***	−0.08	299	n.s	0.12	299	*	0.61	299	***			
Chl. *a* total (μg l^{-1})	−0.28	276	***	−0.24	299	***	0.01	298	n.s	0.39	298	***	0.64	***	298
Chl. *a* $>10\,\mu m$ (μg l^{-1})	−0.26	197	***	−0.31	215	***	0.02	214	n.s	0.45	214	***	0.61	***	214
Chl. *a* 2–10 μm (μg l^{-1})	−0.24	197	***	−0.14	215	*	0.15	214	*	0.58	214	***	0.64	***	214
Chl. *a* $<2\,\mu m$ (μg l^{-1})	0.00	197	n.s	0.04	214	n.s	0.30	213	***	0.58	213	***	0.52	***	213

Correlation coefficient (*r*), $p<0.05$*, $p<0.01$**, $p<0.001$***, not significant (n.s).

Table 10
Mann-Whitney U-test to compare the ratio of NO_3^-/PO_4^{3-}, and salinity concentration in the upwelling area and off the front above the nutricline

	Median	Min	Max	*n*	*t*	*p*
Groups (NO_3^-/PO_4^{3-})						
Upwelling	9.8	1.6	36.0	103	12767	n.s
Off the front	11.8	0.22	37.9	163		
Groups (salinity)						
Upwelling	37.1	36.4	38.1	103	20131	***
Off the front	36.6	36.3	37.4	163		

Median, minimum (Min.), maximum (Max.), number of samples (*n*), *t*-value (*t*). Not significant (n.s), $p<0.001$***.

depleted in phosphate relative to nitrate. The change of N:P ratio from values higher than 16 in potentially upwelling, more saline water to values lower than 16 in upwelled water (Table 10) suggests a fast incorporation and accumulation of nitrate by phytoplankton, especially eukaryotic cells $>2\,\mu m$ were usually found next to the upwelled AMI, where the nutrient availability was higher. Among them, cells $>10\,\mu m$ are mainly responsible for the high Chl *a* concentrations at the upwelling area, which is in agreement to Chisholm (1992) assertion that Chl *a* concentrations higher than certain threshold values ($2\,\mu g\,l^{-1}$) can only occur with the help of large cells.

The main difference between both sides of the front is the marked SSCM at the coastal side of the front. At other frontal systems the highest Chl *a* values have been reported both at the coastal side of the front (Gieskes and Kraay, 1986; Montegut and Raimbault, 1994; Estrada et al., 1999) and off the front (Pingree et al., 1976; Delgado et al., 1992; Raimbault et al., 1993), related to the frequency of mixing events (ranging from tidal to seasonal variability) and the intensity of the upwelling. Thus, in the NW-Alboran Sea, the time-scale for upwelling of deeper water and its advection towards the front in the photic zone appears to be sufficiently long to permit the development of phytoplankton and SSCM.

Our spatial and temporal distribution of Chl *a* (highest in the upwelling area and during the December cruise) agrees with the spatio-temporal variability of sea surface pigment distribution described by García-Górriz and Carr (1999). The authors mention that phytoplankton bloom occurs at minimum incident PAR levels during the annual cycle and suggest that phytoplankton growth is not light limited in the Alboran Sea.

On the other hand, Morán and Estrada (2001) show no significant correlation between primary production and integrated Chl *a* for a very close area of the NW Alboran Sea, although usually a correlation is found between surface and integrated Chl *a* values. They suggest severe light limitation and low contribution of the phytoplankton cells found at subsurface depths, which contained an important proportion of the total Chl *a* in the water column.

Our data show significantly lower C:Chl *a* ratio and higher fluorescence per cell during December (Tables 5 and 6). Biomass at the SSCM in the upwelling area was lowest at this time ($44–111\,mgC\,m^{-3}$) while the other two cruises April and July exhibited concentration between 126 and $251\,mgC\,m^{-3}$ (Table 4). Avoiding the influence of vertical position of the SSCM, cell volume and biomass conversion factors; an ANOVA and posthoc test (tukey) on integrated (0–100 m) abundances determined by flow cytometry (cells $<20\,\mu m$) was carried out for the upwelling area, which demonstrate significantly lower abundances in December ($68\pm 49\times10^6\,cells\,cm^{-2}$, $n=7$) than in June ($189\pm46\times10^6\,cells\,cm^{-2}$, $n=3$) and April 1996 ($190\pm21\times10^6$ cells cm^{-2}, $n=7$). All these

findings suggest photoacclimation of phytoplankton to either lower incident irradiance in the upwelling area in winter without nutrient limitation (Fig. 5), or longer residence time of the cells in deeper water due to increasing mixing depth in winter, and support the necessity of improving coupled in situ and remote sensing studies.

With respect to picoplankton, the eukaryotic fraction was ubiquitous but the prokaryotic *Prochlorococcus* and *Synechococcus* reached the highest abundance associated to the impoverished MAW off the front, which is consistent to the spatial covariation of both prokaryotes described by Vaulot and Partensky (1990), and Binder et al. (1996). Consequently, *Prochlorococcus* and *Synechococcus* presented significant positive correlations with temperature, water column stability and the distance to the interface (AMI) which turns into the opposite for cells $>2\,\mu m$ (Table 9). No correlation was found between prokaryotic phytoplankton abundance and Chl *a* concentration $<2\,\mu m$, perhaps because *Prochloroccoccus* is most abundant in well illuminated surface water and exhibit lower C:Chl *a* ratio as indicated by the low fluorescence $cell^{-1}$ ratio.

Related to these observations, the analysis of the abundance of *Prochlorococcus*, *Synechococcus* and eukaryotic picoplankton at the neighbour Almería-Oran front, allowed Jacquet et al. (2002) to distinguish two major types of systems: (a) mesotrophic conditions (Atlantic waters, detectable nutrient level) dominated by eukaryotes and *Synechococcus*, and (b) more oligotrophic areas (Mediterranean sea waters, low to undetectable nutrient levels) dominated by *Prochlorococcus* and, to a lesser extent, *Synechococcus*. A similar association is suggested by Partensky et al. (1996) and Zubkov et al. (1998) in the NW-African upwelling area. Such association could only be suggested for our data on a seasonal scale: *Synechococcus* with mesotrophic (spring) waters and *Prochlorococcus* associated with potentially more oligotrophic (summer) waters. The maximum abundance of *Prochlorococcus* found in this study ($6.2\times10^4\,cells\,ml^{-1}$) was similar to those described previously for the Mediterranean Sea (Vaulot and Partensky, 1990; Li et al., 1993; and Zohary et al., 1998) and were considerably lower than those described for the Atlantic Ocean ($10–28\times10^4\,cells\,ml^{-1}$, Olson et al., 1990; Veldhuis and Kraay, 1993; Zubkov et al., 1998).

Upwelling processes fuel phytoplankton growth in general but especially that of large cells (Malone, 1980). According to this, Rodríguez et al. (1998) described significantly flatter size-spectra under cyclonic than under anticyclonic circulation in the Alboran Sea. Correspondingly, in this study the higher phytoplanktonic biomass dominated by cells $>2\,\mu m$ found in the upwelling area resulted in flatter size-spectra than off the front. The injection of nutrients into the photic layers associated to the vertical motion produced by the upwelling is the usual explanation for the growth of large cells in these areas (Arin et al., 2002). However, Rodríguez et al. (2001) demonstrate a direct relationship between phytoplankton size-distribution and vertical velocity with no dependence on nutrient availability, where positive vertical velocities in part counteract the size-dependent sedimentation velocities.

Although in the present study it is not possible to determine the importance of each mechanism to the abundance of big cells, the flatter size-spectra usually found in the upwelling area will have important implications for the fate of phytoplankton biomass in the region (in the sense of Legendre and Le Fèvre, 1989). The encountered north–south displacement of the front alternates DU during the southward drift and subduction of upwelled waters during the northward drift, which may enhance along isopycnal export of phytoplankton, in a similar way as depicted by Fiedling et al. (2001) in the close Almería-Oran front. The almost permanent or periodical mesoscale fertilizing events may influence basin-wide balances established on macroscale studies. More intensive mesoscale studies with accurate estimations of upwelling rates and vertical velocities together with process measurements like primary production, nitrate uptake, underwater light fields, size-structures and export of biomass to the sea floor would be necessary to improve our understanding about the exploitable and exportable biomass in small but high-dynamic regions like the Alboran Sea.

Acknowledgements

This study was financed by the Spanish CICYT Project MAR-95-1950-CO2-02. The Instituto Español de Oceanografía (IEO) also collaborated in this study. We thank the crew of R.V. "Odón de Buen" (I.E.O.) for their effort during the cruises, and J. Escánez (I.E.O., Santa Cruz de Tenerife) for nutrient analysis assistance. First author A. R. was also supported by the EU Project "Canary Islands and Açores Gibraltar Observations".

References

Arin, L., Morán, X.A.G., Estrada, M., 2002. Phytoplankton size distribution and growth rates in the Alboran Sea (SW Mediterranean): short-term variability related to mesoscale hydrodynamics. Journal of Plankton Research 24, 1019–1033.

Baldacci, A., Corsini, G., Grasso, R., Manzella, G., Allen, J.T., Cipollini, P., Guymer, T.H., Snaith, H.M., 2001. A study of the Alboran sea mesoscale system by means of empirical orthogonal function decomposition of satellite data. Journal of Marine Systems 29, 293–311.

Binder, B.J., Chisholm, S.W., Olson, R.J., Frankel, S.I., Worden, A.Z., 1996. Dynamics of picophytoplankton, ultraplankton and bacteria in the central equatorial Pacific. Deep-Sea Research II 43 (4–6), 907–931.

Bormans, M., Garrett, C., 1989. A simple criterion for gyre formation by the surface outflow from a strait, with application to the Alboran Sea. Journal of Geophysical Research 94, 12637–12644.

Bryden, H.L., Kinder, T.H., 1991. Steady two-layer exchange through the Strait of Gibraltar. Deep-Sea Research 38 (1), S445–S463.

Cano, N., 1978. Resultados de la campaña Alborán 76. Boletín Instituto Español de Oceanografía 247, 3–50.

Chisholm, S.W., 1992. Phytoplankton size. In: Falkowski, P.G., Woodhead, A.D. (Eds.), Primary Productivity and Biogeochemical Cycles in the Sea. Plenum Press, New York, pp. 213–237.

Chisholm, S.W., Olson, R.J., Zettler, E.R., Goericke, R., Waterbury, J., Welschmeyer, N., 1988. A novel free-living prochlorophyte abundant in the oceanic euphotic zone. Nature 334, 340–343.

Delgado, M., Latasa, M., Estrada, M., 1992. Variability in the size-fractionated distribution of the phytoplankton across the Catalan front of the north-west Mediterranean. Journal of Plankton Research 14 (5), 753–771.

Dugdale, R.C., Goering, J.J., 1967. Uptake of new and regenerated forms of nitrogen in primary productivity. Limnology and Oceanography 12, 196–206.

Echevarría, F., Lafuente, J.G., Bruno, M., Gorsky, G., Goutx, M., González, N., García, C.M., Gómez, F., Vargas, J.M., Picheral, M., Striby, L., Varela, M., Alonso, J.J., Reul, A., Cózar, A., Prieto, L., Sarhan, T., Plaza, F., Jiménez-Gómez, F., 2002. Physical-biological coupling in the Strait of Gibraltar. Deep-Sea Research II 49, 4115–4130.

Estrada, M., Varela, R.A., Salat, J., Cruzado, A., Arias, E., 1999. Spatio-temporal variability of the winter phytoplankton distribution across the Catalan and North Balearic fronts (NW Mediterranean). Journal of Plankton Research 21 (1), 1–20.

Fabres, J., Calafat, A., Sánchez-Vidal, A., Canals, M., Heussner, S., 2002. Composition and spatio-temporal variability of particle fluxes in the Western Alboran Gyre, Mediterranean Sea. Journal of Marine Systems 33–34, 431–456.

Fanning, K.A., 1992. Nutrient provinces in the Sea: concentration ratios, reaction rate ratios, and ideal covariation. Journal of Geophysical Research 97, 5693–5712.

Fiedling, S., Crisp, N., Allen, J.T., Hartman, M.C., Rabe, B., Roe, H.S.J., 2001. Mesoscale subduction at the Almería-Oran front part 2. Biophysical interactions. Journal of Marine Systems 30, 287–304.

García-Górriz, E., Carr, M-E., 1999. The climatological annual cycle of satellite-derived phytoplankton pigments in the Alboran Sea. Geophysical Research Letters 26 (19), 2985–2988.

García-Lafuente, J., Cano, N., Vargas, M., Rubín, J.P., Hernández-Guerra, A., 1998. Evolution of the Alboran Sea hydrographic structures during July 1993. Deep-Sea Research I 45, 39–65.

García-Lafuente, J., Sarhan, T., Vargas, M., Vargas, J.M., Plaza, F., 1999. Tidal motions and tidally induced fluxes through La Linea submarine canyon, western Alboran Sea. Journal of Geophysical Research 104, 3109–3119.

Gascard, J.C., Richez, C., 1985. Water masses and circulation in the western Alboran Sea and Strait of Gibraltar. Progess in Oceanography 15, 157–216.

Gieskes, W.W.C., Kraay, G.W., 1986. Floristic and physiological differences between the shallow and deep nanophytoplankton community in the euphotic zone of the open tropical Atlantic revealed by HPLC analysis of pigments. Marine Biology 91, 567–576.

Green, R.E., Sosik, H.M., Olson, R.J., DuRand, M.D., 2003. Flow cytometric determination of size and complex refractive index for marine particles: comparison with independent and bulk estimates. Applied Optics 42 (3), 526–541.

Heburn, S., La Violette, P.E., 1990. Variations in the structure of the anticyclonic gyres found in the Alboran Sea. Journal of Geophysical Research 95, 1599–1613.

Jacquet, S., Prieur, L., Avois-Jacquet, C., Lennon, J.-F., Vaulot, D., 2002. Short-timescale variability of picophytoplankton abundance and cellular parameters in surface waters of the Alboran Sea (western Mediterranean). Journal of Plankton Research 24 (7), 635–651.

Jiménez-Gómez, F., 1995. Estructura de tamaños y dinámica del ultraplancton en el ecosistema pelágico. Ph.D. Thesis, University of Málaga, Spain, unpublished.

Kana, T.M., Glibert, P.M., 1987. Effect of irradiance of up to 2000 $\mu E\,m^{-2}\,s^{-1}$ on marine Synechococcus WH7803. 1. Growth, pigmentation and cell composition. Deep-Sea Research 34, 479–495.

Krom, M.D., Kress, N., Brenner, S., Gordon, L.I., 1991. Phosphorus limitation of primary productivity in the eastern Mediterranean Sea. Limnology and Oceanography 36 (3), 424–432.

La Violette, P.E., 1984. The advection of cyclic submesoscale thermal features in the Alboran Sea Gyre. Journal of Physical Oceanography 14 (3), 550–565.

Legendre, L., Le Fèvre, J., 1989. Hydrodynamical singularities as controls of recycled versus export production in oceans. In: Berger, W.H., Smetacek, V.S., Wefer, G. (Eds.), Productivity in the Ocean: Present and Past. Wiley, Chichester, pp. 49–63.

Li, W.K.W., Dickie, P.M., Irwin, B.D., Wood, A.M., 1992. Biomass of bacteria, cyanobacteria, prochlorophytes and photosynthetic eukaryotes in the Sargasso Sea. Deep-Sea Research 39, 501–519.

Li, W.K.W., Zohary, T., Yacobi, Y.Z., Wood, A.M., 1993. Ultraplankton in the eastern Mediterranean Sea: towards deriving phytoplankton biomass from flow cytometric measurements of abundance, fluorescence and light scatter. Marine Ecology Progress Series 102, 79–87.

Malone, T.C., 1980. Algal size. In: Morris, I. (Ed.), The Physiological Ecology of Phytoplankton. Blackwell Scientific Publications, Oxford, pp. 133–463.

Menden-Deuer, S., Lessard, E.J., 2000. Carbon to volume relationships for dinoflagellates, diatoms and other protist plankton. Limnolgy and Oceanography 45 (3), 569–579.

Minas, H.J., Minas, M., Packard, T.T., 1986. Productivity in upwelling areas deduced from hydrographic and chemical fields. Limnology and Oceanography 31 (6), 1182–1206.

Montegut, C.C., Raimbault, P., 1994. The Peruvian upwelling near 15°S in August 1986. Results of continuous measurements of physical and chemical properties between 0–200 m depth. Deep-Sea. Research I 41 (3), 439–467.

Morán, X.A.G., Estrada, M., 2001. Short-term variability of photosynthetic parameters and particulate and dissolved primary production in the Alboran Sea (SW Mediterranean). Marine Ecology Progress Series 212, 53–67.

Morán, X.A., Taupier-Letage, I., Vázquez-Domínguez, E.,S., Arin, L., Raimbault, P., Estrada, M., 2001. Physical–biological coupling in the Algerian Basin (SW Mediterranean): influence of mesoscale instabilities on the biomass and production of phytoplankton and bacterioplankton. Deep-Sea Research I 48, 405–437.

Morel, A., André, J.M., 1991. Pigment distribution and primary production in the western Mediterranean as derived and modelled from coastal zone colour scanner observations. Journal of Geophysical Research 96 (C7), 12685–12698.

Morel, A., Ahn, Y.-H., Partensky, F., Vaulot, D., Claustre, H., 1993. Prochlorococcus and Synechococcus: a comparative study of their optical properties in relation to their size and pigmentation. Journal of Marine Research 51, 617–649.

Olson, R.J., Chisholm, S.W., Zettler, E.R., Altabet, M.A., Dusenberry, J.A., 1990. Spatial and temporal distributions of prochlorophyte picoplankton in the North Atlantic Ocean. Deep-Sea Research 37 (6), 1033–1051.

Parada, M., Cantón, M., 1998. The spatial and temporal evolution of thermal structures in the Alboran Sea Mediterranean basin. International Journal of Remote Sensing 19, 2119–2131.

Partensky, F., Blanchot, J., Lantoine, F., Neveux, J., Marie, D., 1996. Vertical structure of picophytoplankton at different trophic sites of the tropical Northeastern Atlantic Ocean. Deep-Sea Research I 43 (8), 1191–1213.

Pingree, R.D., Holligan, P.M., Mardell, G.D., Head, R.N., 1976. The influence of physical stability on spring summer and autumn phytoplankton blooms in the Celtic Sea. Journal of the Marine Biological Association of the United Kingdom 56, 845–873.

Prieur, L., Sournia, A., 1994. Almofront-1 (April–May 1991): an interdisciplinary study of the Almeria–Oran geostrophic front, SW Mediterranean Sea. Journal of Marine Systems 5, 187–203.

Raimbault, P., Coste, B., Boulhadid, M., Boudjellal, B., 1993. Origin of high phytoplankton concentration in deep chlorophyll maximum (DCM) in a frontal region of the southwestern mediterranean sea (algerian current). Deep-Sea Research I 40 (4), 791–804.

Reul, A., Vargas, J.M., Jiménez-Gómez, F., Echevarría, F., García-Lafuente, J., Rodríguez, J., 2002. Exchange of planktonic biomass through the Strait of Gibraltar in late summer conditions. Deep-Sea Research II 49, 4131–4144.

Rodríguez, V., Blanco, J.M., Jiménez-Gómez, F., Rodríguez, J., Echevarría, F., Guerrero, F., 1997. Distribución espacial de algunos estimadores de biomasa fitoplanctónica y material orgánico particulado en el mar de Alborán, en condiciones de estratificación térmica (Julio de 1993). Publicación Especial Instituto Español Oceanografía 24, 53–64.

Rodríguez, J., Blanco, J.M., Jiménez-Gómez, F., Echevarría, F., Gil, J., Rodríguez, V., Ruíz, J., Bautista, B., Guerrero, F., 1998. Patterns in the size structure of the phytoplankton community in the deep fluorescence maximum of the Alboran Sea (southwestern Mediterranean). Deep-Sea Research I 45, 1577–1593.

Rodríguez, J., Tintoré, J., Allen, J.T., Blanco, J.M., Gomis, D., Reul, A., Ruíz, J., Rodríguez, V., Echevarría, F., Jiménez-Gómez, F., 2001. Mesoscale vertical motion and the size structure of phytoplankton in the ocean. Nature 410, 360–363.

Rodríguez, J., Jiménez-Gómez, F., Blanco, J.M., Figueroa, F.L., 2002. Physical gradients and spatial variability of the size structure and composition of phytoplankton in the Gerlache Strait (Antarctica). Deep-Sea Research II 49, 693–706.

Ruíz, J., Echevarría, F., Font, J., Ruíz, S., García, E., Blanco, J.M., Jiménez-Gómez, F., Prieto, L., González-Alaminos, A., García, C.M., Cipollini, P., Snaith, H., Bartual, A., Reul, A., Rodríguez, V., 2001. Surface distribution of

chlorophyll, particles and gelbstoff in the Atlantic jet of the Alborán Sea: from submesoscale to subinertial scales of variability. Journal of Marine Systems 29, 277–292.

Sarhan, T., García-Lafuente, J., Vargas, M., Vargas, J.M., Plaza, F., 2000. Upwelling mechanisms in the Northerwestern Alboran Sea. Journal of Marine Systems 23, 317–331.

Strickland, J.D.H., Parsons, T.R., 1972. A Practical Handbook of Sea Waters Analysis. second ed. Bulletin of Fish Research Bd, Canada, vol. 167, 310 pp.

Thingstad, T.F., Zweifel, L.U., Rassoulzadegan, F., 1998. P limitation of heterotrophic bacteria and phytoplankton in the northwest Mediterranean. Limnology and Oceanography 43 (1), 88–94.

Tintoré, J., La Violette, P.E., Blade, I., Cruzado, A., 1988. A study of an intense density front in the Eastern Alboran Sea: the Almeria-Oran Front. Journal of Physical Oceanography 18, 1384–1397.

Tintoré, J., Gomis, D., Alonso, S., Parrilla, G., 1991. Mesoscale Dynamics and Vertical Motion in the Alborán Sea. Journal of Physical Oceanography 21 (6), 811–823.

Utermöhl, H., 1958. Zur Vervollkommnung der quantitativen Phytoplankton-Methodik. Mitteilungen/Internationale Vereinigung für Theoretische und Angewandte Limnologie 9, 1–38.

Vargas-Yáñez, M., Plaza, F., García-Lafuente, J., Sharan, T., Vargas, J.M., Vélez-Belchi, P., 2002. About the seasonal variability of the Alboran Sea circulation. Journal of Marine Systems 35, 229–248.

Vaulot, D., Partensky, F., 1990. Winter presence of prochlorophytes in surface waters of the Northwestern Mediterranean Sea. Limnology and Oceanogrphy 35 (5), 1156–1167.

Vaulot, D., Courties, C., Partensky, F., 1989. A simple method to preserve oceanic phytoplankton for flow cytometric ananlysis. Cytometry 10, 629–635.

Veldhuis, M.J.W., Kraay, G.W., 1993. Cell abundance and fluorescence in relation to growth irradiance and nitrogen availability in the Red Sea. Netherland Journal of Sea Research 31 (2), 135–145.

Verity, P., Robertson, C.Y., Tronzo, C.R., Andrews, M.G., Nelson, J.R., Sieracki, M.E., 1992. Relationship between cell volume and carbon and nitrogen content of marine photosynthetic nanoplankton. Limnology and Oceanography 37 (7), 1434–1446.

Viúdez, A., Tintoré, J., Haney, R.L., 1996. Circulation in the Alboran Sea as determined by quasi-synoptic hydrographic observations. Part I: Three-dimensional structure of the two anticyclonic gyres. Journal of Physical Oceanography 26 (5), 684–705.

Yentsch, C.M., Menzel, D., 1963. A method for the determination of phytoplankton chlorophyll and phaeophytin by fluorescence. Deep-Sea Research 63 (10), 221–231.

Zohary, T., Brenner, S., Krom, M.D., Angel, D.L., Kress, N., Li, W.K.W., Neoro, A., Yacobi, Y.Z., 1998. Build-up of microbial biomass during deep winter mixing in a Mediterranean warm-core eddy. Marine Ecology Progress Series 167, 47–57.

Zubkov, M.V., Sleigh, M.A., Tarran, G.A., Burkill, P.H., Leakey, R.G.J., 1998. Picoplanktonic community structure on Atlantic transect from 50ºN to 50ºS. Deep-Sea Research I 45, 1339–1355.